Hydrodynamics and electrokinetics of spherical liposomes with coatings of terminally anchored poly(ethylene glycol): Numerically exact electrokinetics with self-consistent mean-field polymer

Reghan J. Hill*
Department of Chemical Engineering, McGill University Montreal, Quebec, Canada H3A2B2
(Received 22 December 2003; revised manuscript received 8 July 2004; published 30 November 2004)

A detailed theoretical model is presented to interpret electrokinetic experiments performed on colloids with uncharged polymer layers. The methodology removes many of the degrees of freedom that otherwise have to be accounted for by adopting multiple empirical fitting parameters. Furthermore, the level of detail provides a firm basis for future studies examining liposome surface chemistry and charge, surface-charge mobility, and the dynamics of adsorbed polymer on fluidlike membranes. The model predictions are compared with experimental measurements of the electrophoretic mobility of *stealth* liposomes with molecular weights of terminally anchored poly(ethylene glycol) (PEG) in the range $0.35-10\ \mathrm{kg\,mol^{-1}}$ [J. A. Cohen and V. A. Khorosheva, Colloids Surf. A **195**, 113 (2001)]. The experimental data are interpreted by drawing upon self-consistent mean-field calculations of the polymer segment density distributions and numerically exact solutions of the governing transport equations [R. J. Hill, D. A. Saville, and W. B. Russel, J. Colloid Interface Sci. **258**, 56 (2003)]. The approach leads to excellent agreement between theory and experiment with one adjustable parameter—the hydrodynamic size (Stokes radius) $a_s \approx 0.175$ Å of the *statistical* PEG segments with (Kuhn) length $l = 7.1$ Å. The remarkably small Stokes radius is demonstrated to be consistent with other applications of the well-known Debye-Brinkman model and, consequently, this work reveals important limitations of the mean-field hydrodynamic model. Despite such limitations, the "full" electrokinetic model is robust in its predictive capacity. The molecular weights of the terminally anchored PEG span the range where the coatings undergo a transition from mushroomlike to brushlike conformations, and the hydrodynamic size and electrophoretic mobility of the liposomes are demonstrated to be sensitive to the PEG chain length and the effects of double-layer polarization.

DOI: 10.1103/PhysRevE.70.051406 PACS number(s): 82.70.Dd, 87.68.+z

I. INTRODUCTION

Poly(ethylene glycol) (PEG) chains with hydrophobic end groups have found widespread use as coatings for lipid bilayer membranes, as have longer poly(ethylene oxide) (PEO) homopolymers for latices.[1] In biomedical applications, PEG coatings are used to help control (extend) the circulation time of drug-carrying liposomes, often referred to as *stealth liposomes*. PEG layers are also known to inhibit the adsorption of proteins (antibodies), thereby "protecting" the drug carrier from recognition by the immune system.

Synthetic lipid bilayers are an ideal model system for studying polymeric interfaces. This is due, in part, to the high degree of control that can be exercised over the polymer grafting density and, hence, the *steric* contribution to the interaction potential. Similarly, the *electrostatic* contribution can be "tuned" by varying the stoichiometric ratio of charged to uncharged lipids used in the liposome synthesis. In principle, the liposome size can also be controlled and, hence, the effects of surface curvature on the polymer conformation can be realized.

A novel means of studying lipid bilayer surfaces is to support them on monodisperse microspheres. Galnedar and co-workers [1] recently used a novel combination of optical trapping and microelectrophoresis to study enzyme kinetics on "bare" lipid bilayers supported on a silica microsphere. While it is not yet clear that the bilayer surface characteristics are independent of the underlying solid support, the dynamics of the surface charge density and, hence, the reaction kinetics can be characterized. This approach provides new opportunities for studying how charged and uncharged polymers regulate protein adsorption, for example.

The principle challenge in interpreting such experiments lies in quantitatively connecting the measured quantities (electrophoretic mobility and hydrodynamic radius) to surface characteristics. To this end, Brooks and co-workers have developed and applied a variety of continuum electrokinetic models to interpret the electrophoretic mobility of human erythrocytes [2,3], vesicles [4], and liposomes [5]. These models have played an important role in quantitatively characterizing the polymer-coated surfaces of the respective biologically relevant colloids. An important limitation of these models is, perhaps, that the polymer segment density distributions are assumed to be steplike, i.e., the layers are uniform. The models are also limited to flat interfaces, which provides a reasonable approximation for colloids with radius greater than 1 μm at physiological ionic strengths. It is well known, however, that surface curvature is important when the diffuse double-layer thickness is comparable to or greater than the particle radius. These conditions prevail for therapeutic liposomes, which have radii of the order of 100 nm, as

*Electronic address: reghan.hill@mcgill.ca

[1]PEG and PEO chains need only be distinguished by the monomer used to synthesize them.

well as for PEG-derivatized proteins. Such limitations restrict the theoretical interpretation of electrokinetic experiments to high ionic strengths, whereas electrokinetic phenomena are often much richer when viewed over a range of ionic strengths, when the double-layer thickness traverses the characteristic thickness of the polymer layer (see [6]).

The goal of this work is to bring together recent theoretical and computational advances in electrokinetic transport phenomena with a rigorous theoretical description of inhomogeneous polymer layers and to use this theory to interpret relatively well-characterized experiments by Cohen and Khorosheva (CK) measuring the electrophoretic mobility of liposomes with coatings of terminally anchored PEG [7].

The structure of adsorbed polymer layers depends, in part, on the polymer chain length and flexibility, as characterized by the number N and (Kuhn) length l of the *statistical* segments. Also important is the number of grafted chains per unit area, referred to here as the grafting density $\sigma=d^{-2}$, where d is the characteristic distance between the points of attachment. In contrast to layers of adsorbed homopolymer, the structure of terminally anchored layers depends on the chains possessing a relatively short anchoring block or subchain.

The anchoring block for the PEG chains addressed in this work is a terminal (anionic) lipid, phosphatidylethanolamine (PE). This macromolecule has the same (single negative) charge at the PE-PEG link as the phosphatidylglycerol (PG) lipids that contribute to the surface charge of an otherwise neutral membrane composed of (zwitterionic) phosphatidylcholine (PC) lipids. This ensures that the bare and PEG-coated liposomes used in CK's experiments have the same surface charge. In this study, the uncoated liposomes are treated as bare impenetrable spheres, and the *standard electrokinetic model* [8,9] is used to establish the *effective* surface charge from measured electrophoretic mobilities. Then, a rigorous electrokinetic transport model [6] and a self-consistent mean-field description of the polymer layers are used to calculate the effect of PEG on the hydrodynamic size and electrophoretic mobility.

When the grafting density is low and, hence, d is greater than the characteristic coil size lN^{ν}, with $\nu=0.5$ for chains in a *theta* solvent and $\nu\approx 3/5$ for an *athermal* or *good* solvent [10], terminally anchored chains adopt "mushroom" conformations. The nominal coating thickness is then $L' \sim lN^{\nu}$ with nominal segment volume fraction $\phi=nl^3\sim\sigma l^2 N^{1-\nu}$, where n is the segment number density. When the grafting density is high and, hence, d is less than lN^{ν}, the chains are forced to interpenetrate. Excluded volume causes the chains to extend, giving rise to brushlike conformations with $L' \sim Nl(\sigma l^2)^{(1-\nu)/(2\nu)}$ and $\phi\sim(\sigma l^2)^{3/2-1/(2\nu)}$. The "blob" model adopted by de Gennes [11] to arrive at the foregoing *scaling* theories for *planar* brushes has been extended by Daoud and Cotton [12] and others [13,14] to account for highly curved interfaces and charged polymer.

Models that go beyond scaling theory have been developed to account for the effects of surface curvature, the "strength" of the solvent, and the distributions of segments and chain ends. These are based on self-consistent fields, such as the Dolan-Edwards self-consistent mean-field *continuum* theory [15] and the Scheutjens-Fleer self-consistent mean-field *lattice* theory [16]. There exist analytical [13,14,17–20] and numerically exact [13,21–23] solutions of various mean-field models for neutral polymer brushes. It should also be mentioned here that there exists a large body of literature devoted to charged (polyelectrolyte) layers (e.g., [24–27]).

Mention should also be made of more direct calculations, using Monte Carlo [28–31] and Brownian dynamics [32–34] simulations, which address equilibrium and dynamic aspects, respectively. In general, there exists good agreement between mean-field theories and the results of a relatively few direct calculations for neutral polymer brushes. The differences mostly concern details of the region close to the grafting surface and, of course, the various numerical prefactors, or lack thereof, required for quantitative comparisons. The available evidence suggests that mean-field approximations for neutral, grafted chains are satisfactory from an at least semiquantitative point of view.

Coatings of adsorbed PEO chains (homopolymer) are widely used to sterically stabilize colloidal dispersions and can also be used to induce flocculation [35,36]. In contrast to terminally anchored chains, adsorbed homopolymers give rise to a compact inner region, with a low-density outer region comprised of loops and tails. These layers have been studied using (i) ground-state approximations to the solution of self-consistent mean-field equations [37,38] and (ii) self-consistent mean-field lattice theory [39–41].

The foregoing calculations of the equilibrium segment density distribution provide the segment-weighted coating thickness, via moments of the segment density distribution and the hydrodynamic thickness, via Brinkman's equations [42–44]. These can be measured using techniques based on (i) the *scattering* of neutrons and x rays, for example, and (ii) *hydrodynamics*, as interrogated by capillary flow, viscometry, and quasielastic light scattering [16].

In contrast to flows driven entirely by pressure gradients or viscous shear stresses, electrically driven flows are sensitive to the segment density distribution throughout the coating, not just at the periphery. The theoretical interpretation of electrokinetic experiments therefore poses a much more challenging and rigorous test of theory, and there is much more to be learned of the surface and the transport processes that take place there [2,6,45–47].

Despite the extensive literature devoted to the "structure" of polymer layers, the influence of such coatings on the electrokinetics of polymer-coated colloids is not well understood. The nonlinear Poisson-Boltzmann equation and deformation of the diffuse double layer severely limit analytical theory. O'Brien and White's [48] well-known approach to numerically solve the "full" electrokinetic model (standard model) overcame these difficulties for bare colloids, and the boundary conditions have since been modified to account for transport processes taking place in an infinitesimally thin surface layer [49,50]. Nevertheless, when these so-called Stern-layer models are adopted to mimic the effects of surface-bound polymer, the interpretation of experiment remains empirical.

Recently, Hill, Saville, and Russel [6] (HSR) solved the full electrokinetic model for colloids with neutral (uncharged) and charged (polyelectrolyte) polymer coatings. Since the model requires knowledge of the radial distribution

of polymer segments and their hydrodynamic size and charge, it has not yet been applied to quantitatively interpret experiments. Various approximate solutions have been developed, most notably by Ohshima, who set out a general form of the full model and provided analytical solutions for various asymptotic limits, neglecting double-layer polarization (e.g., [51,52]). Earlier, Levine and co-workers [2] used a numerical approach to address the effect of high surface potentials, for large polyelectrolyte-coated colloids (human erythrocytes). Janzen and co-workers [5] applied this model (by setting the polymer charge density to zero) to interpret the electrophoretic mobility of PEG-coated liposomes. More recently, Saville [47] applied a semianalytical approach, pointing out the significance of double-layer polarization for large particles with thin, charged and uncharged polymer layers.

The numerical approach of Janzen *et al.* for uniform, uncharged polymer layers is similar to Ohshima's analytical theory, but the *shear plane* may be displaced from the plane of (surface) charge. The thin region between the charged surface and shear plane is hydrodynamically impermeable, but permits ion diffusion. For flat interfaces, shifting the shear plane out from the plane of (possibly fixed) surface charge lowers the effective surface potential and, hence, lowers the effective surface charge. Janzen *et al.* applied their model to infer the polymer conformation from measured electrophoretic mobilities. Because the layers were assumed uniform and the range of polymer molecular weights was small, their interpretation of experiments was limited in many quantitative respects. Nevertheless, the study clearly highlights the significant effect that neutral polymer has on the electrophoretic mobility and, furthermore, it provides a sound basis for the much more detailed calculations presented below.

In this work, the HSR electrokinetic model is compared with experiment by adopting a self-consistent mean-field theory to calculate the radial distribution of polymer segments. These distributions are used to specify the Brinkman permeability appearing in the electrokinetic model. Cohen and Khorosheva's experiments [7] are sufficiently well characterized that there remains only *one* "unknown" parameter with which to fit the full model over a wide range of PEG molecular weights and bulk ionic strengths. The "fitting" parameter is the hydrodynamic (Stokes) radius of the polymer (statistical) segments, a_s. Therefore, given the polymer grafting density and molecular weight, and the underlying charge density, this work establishes a model to predict the hydrodynamic and electrokinetic characteristics of a variety of spherical colloids with terminally anchored PEG coatings. In principle, the model can be applied to infer the amount of adsorbed polymer and charge from measurements of the electrophoretic mobility, for example. Alternatively, given the polymer grafting density and molecular weight, it provides the effective particle size.

In Sec. II, the HSR electrokinetic model is described, followed by a description of the self-consistent mean-field model for calculating polymer segment density distributions. In Sec. III, CK's experiments with micron-sized PEG-coated liposomes are interpreted using the full theory, thereby establishing the hydrodynamic radius of the statistical polymer segments. The subsections therein discuss the structure, thickness, density, and permeability of the coatings. Section IV addresses the remarkably small hydrodynamic size of the polymer segments. A summary follows in Sec. V.

II. THEORY

The procedure is to first calculate the equilibrium distribution of polymer segments using a self-consistent mean-field theory. Then, the segment density distribution is adopted in the HSR electrokinetic model to specify the Brinkman permeability and, hence, to calculate the effective particle size and electrophoretic mobility. The electrokinetic and self-consistent mean-field models are described below, in Secs. II A and II C, respectively. Section II B links the electrokinetic model to the effective coating thickness and electrophoretic mobility.

A. Continuum electrokinetic model

An impermeable spherical colloid is suspended in an unbounded electrolyte. The particle surface is characterized by a uniform distribution of charge or surface potential, and attached to the surface is a radially varying distribution of polymer segments. In general, a fraction of the polymer segments may be charged, and the polymer and underlying surface charge may vary with the bulk electrolyte concentration. In this work, however, the polymer is neutral and the surface charge is assumed constant. At equilibrium, i.e., in the absence of buoyancy and applied electric fields, the particle develops a spherically symmetric diffuse double layer. Then, with the application of an electric field, the particle is set in motion with a velocity that reflects characteristics of the electrolyte, polymer coating, and particle.

The electrostatic potential is coupled to the distribution of charge by the well-known Poisson-Boltzmann equation

$$\nabla^2\psi = -\sum_{j=1}^{N} z_j n_j, \tag{1}$$

where the potential ψ is scaled with the thermal energy per elementary charge kT/e, and z_j denote the valence of the jth ion species. The densities of the counterions n_j, which contribute to the net charge density in the electrolyte, are scaled with twice the ionic strength

$$2I = \sum_{j=1}^{N} z_j^2 n_j^\infty, \tag{2}$$

where n_j^∞ denotes ion densities in the bulk electrolyte. For a 1-1 electrolyte, the scaled ion densities decay to $n_1^\infty/(2I) = n_2^\infty/(2I) = 0.5$ in the bulk, for example. Throughout this section, lengths are scaled with the double-layer thickness

$$\kappa^{-1} = \sqrt{kT\epsilon_s\epsilon_0/(2Ie^2)}, \tag{3}$$

where ϵ_s is the dielectric constant of the solvent and ϵ_0 is the permittivity of free space. For an aqueous solvent at room temperature, the double-layer thickness is typically less than 100 nm.

The ion transport equations are

$$N_{\mathrm{Pe}_j}(\boldsymbol{u}-\boldsymbol{v}_j)-z_j\nabla\psi-\nabla\ln(n_j)=\mathbf{0}\ (j=1,\ldots,N), \quad (4)$$

where the fluid and ion velocities $\boldsymbol{u}$ and $\boldsymbol{v}_j$ are scaled with a characteristic velocity

$$u^*=\epsilon_s\epsilon_0(kT/e)^2/(\eta a). \quad (5)$$

Here, a is the "bare" particle radius and η is the solvent viscosity. For particles with $a=100$ nm in an aqueous solvent, $u^*\sim 10^{-3}$ ms^{-1}, and with ion diffusivities $D_j \sim 10^{-9}$ m^2 s^{-1}, the ion Péclet numbers

$$N_{\mathrm{Pe}_j}=u^*\kappa^{-1}/D_j \quad (6)$$

are $O(10^{-1}/(\kappa a))$; these indicate the extent to which convection may deform the equilibrium double layer. Note that the ion diffusivities $D_j=kT/\lambda_j$ may be obtained from the respective ion mobilities $\lambda_j^{-1}=\Lambda_j/(e^2|z_j|)$, where Λ_j are the limiting conductances for dilute electrolytes [53].

Under steady conditions, the ion conservation equations are

$$\nabla\cdot(n_j\boldsymbol{v}_j)=0\ (j=1,\ldots,N), \quad (7)$$

with fluid momentum and mass conservation governed by the linearized Navier-Stokes equations

$$\nabla^2\boldsymbol{u}-\nabla p-\mathcal{B}(r)(\boldsymbol{u}-\boldsymbol{V})-\kappa a\sum_{j=1}^{N}n_jz_j\nabla\psi=\mathbf{0} \quad (8)$$

and

$$\nabla\cdot\boldsymbol{u}=0. \quad (9)$$

The particle velocity $\boldsymbol{V}$ and the pressure p are scaled with u^* and $\eta u^*\kappa$, respectively. Note that, in setting the third term on the left-hand side of Eq. (8) proportional to $\boldsymbol{u}-\boldsymbol{V}$, the underlying bare particle and the polymer coating are assumed to move together as a rigid composite.

The dimensionless function

$$\mathcal{B}(r)=1/[\kappa\ell(r)]^2 \quad (10)$$

appearing in Eq. (8) is the square of the ratio of the double-layer thickness to the *Brinkman screening length* ℓ, which characterizes the (local) hydrodynamic permeability of the polymer coating. The resulting *Darcy drag force* accounts for hydrodynamic drag arising from the relative motion of the polymer segments and interstitial fluid.

The Brinkman screening length may be related to the structure of the polymer coating by expressing the body force as the product of the polymer segment density $n(r)$ and the drag force on a single segment $f_s=6\pi\eta a_s(u-V)F_s$. When the segments are represented by spheres with (Stokes) radius a_s, the dimensionless drag coefficient F_s depends on the volume fraction $\phi_s=n(4/3)\pi a_s^3$. Equating nf_s to the dimensional form of the Darcy drag term in Eq. (8), $(\eta/\ell^2)(u-V)$, gives

$$\ell^2=1/(n6\pi a_sF_s)=2a_s^2/(9\phi_sF_s). \quad (11)$$

In this work, the *local* distribution of polymer segments is modeled as a rigid "random" configuration of spheres, with a drag coefficient [54,55]

$$F_s=\frac{1+3(\phi_s/2)^{1/2}+(135/64)\phi_s\ln\phi_s+16.456\phi_s}{1+0.681\phi_s-8.48\phi_s^2+8.16\phi_s^3} \quad (12)$$

when the volume fraction is less than approximately 0.4. This formula accounts for drag force on the segments arising from their hydrodynamic interactions. In the dilute limit ($\phi_s\to 0$), which is relevant in this work, Eq. (12) recovers Brinkman's well-known formula [42]. The longer-range inhomogeneity of the coatings is described by the self-consistent mean-field model discussed in Sec. II C.

The surface charge density σ on the bare particle is assumed constant and uniform, and imposes the surface boundary condition

$$\nabla\psi|_+\cdot\boldsymbol{n}-(\epsilon_p/\epsilon_s)\nabla\psi|_-\cdot\boldsymbol{n}=-\sigma \text{ at } r=\kappa a, \quad (13)$$

where ϵ_p is the dielectric constant of the bare particle,[2] and n is an outward unit normal. Here, the surface-charge density is scaled with $\kappa\epsilon_s\epsilon_0kT/e$, and the plus and minus subscripts indicate the solvent and particle sides of the surface, respectively.

If the potential at the surface of the bare particle ζ is specified instead of the surface charge density, then Eq. (13) provides the surface charge density. In the far field, the gradient of the potential approaches the applied electric field, so

$$\psi\to-\boldsymbol{E}\cdot\boldsymbol{r} \text{ as } r\to\infty, \quad (14)$$

where the electric field strength E is scaled with $kT\kappa/e$.

Other surface boundary conditions, which are not discussed here, ensure the impenetrability of the bare particle and the no-slip condition at its surface. The far-field boundary conditions ensure the proper decays of the electrostatic potential, ion densities, and fluid velocity [6].

B. Electrophoretic mobility and hydrodynamic size

The solution of the electrokinetic model presented above is obtained by first solving the nonlinear Poisson-Boltzmann equation for the spherically symmetric equilibrium distributions of ψ and n_j. Then, with the application of a weak uniform electric field $\boldsymbol{E}$ or far-field velocity $\boldsymbol{U}=-\boldsymbol{V}$, there results a system of stiff, linear ordinary differential equations whose solution yields the perturbed electrostatic potential, ion densities, and fluid velocity. As shown in detail by Hill *et al.* [6], the far-field decay of the fluid velocity disturbance, together with the particle equation of motion, leads to the dimensionless *electrophoretic mobility*[3]

$$M=V3\eta e/(E2\epsilon_s\epsilon_0kT) \quad (15)$$

and *drag coefficient*

$$F=f/(6\pi\eta aV), \quad (16)$$

where f is the drag force on the composite particle when it is translated in an unbounded electrolyte with relative velocity

[2]The electrostatic boundary conditions do not affect the electrophoretic mobility [48], so, in this work, the value of ϵ_p is irrelevant.

[3]The magnitude (not the sign) of the mobility is reported.

V in the absence of an applied electric field. In this work, the drag coefficient is interpreted by adopting an *effective coating thickness*

$$L = a(F - 1), \tag{17}$$

where $a+L$ is the radius of a bare uncharged sphere with the same drag coefficient as the charged coated sphere under consideration. Note that $L>0$ because of (i) the hydrodynamic drag of the polymer segments and (ii) electroviscous drag due to electro-osmosis of mobile charge within the diffuse double layer [56]. In the absence of electroviscous effects, the effective coating thickness equals the *hydrodynamic* coating thickness. The "actual" thickness of a steplike (uniform) coating or the characteristic thickness of a nonuniform coating is denoted L'.

C. Self-consistent mean-field theory

The electrokinetic model described briefly above requires knowledge of the radial distribution of polymer segments which, in turn, specify the spatially varying Brinkman permeability. In previous applications of the model and in its various simplified forms, the segment density distribution has been assumed step like [2,45,47,51], exponentially decaying [51], or diffuse [6].

This section describes a methodical approach for calculating the segment density distribution for terminally anchored chains. The density is calculated from knowledge of fundamental characteristics, such as the segment size l, the number of statistical segments, N, and the grafting density σ. The approach is similar to the well-known lattice models of Fleer *et al.* [16] but the *continuum* approach adopted here is closer to that of Dolan and Edwards [15] and the more recent calculations of Dan and Tirrel [21] for curved interfaces.

The probability of a chain beginning at radial position r' and ending at r in s steps, with each step of length l, is denoted $G(r,r',s)$. When this probability varies slowly on the segment length scale, under the influence of an "external" potential $U(r)$, it evolves according to [15,57]

$$\frac{\partial G}{\partial s} = \frac{l^2}{6}\nabla^2 G + [1 - e^{U(r)/(kT)}]G. \tag{18}$$

In the *mean-field* approximation adopted in this work, U is to be determined self-consistently and is therefore expressed in terms of the (local) segment density n, which is often referred to in terms of a volume fraction

$$\phi = n(r)l^3, \tag{19}$$

where l is the length of a segment. The contour length is $l_c = Nl$, where N is the number of statistical segments per chain. These statistical parameters are related to the number of monomer segments or degree of polymerization in Sec. III B.

The self-consistent mean-field potential adopted in this work is obtained following Patttanayek and Juvekar's analysis, which, in turn, rests upon Flory's well-known theory for homogeneous polymer solutions. According to the Flory theory, the free energy of mixing $V_m n_2/N$ polymer chains with $V_m n_1$ solvent molecules is

$$F/(kT) = V_m n_1 \ln \phi_1 + V_m n_2 \frac{1}{N}\ln(\phi_2) + \chi(\phi_2,T)V_m n_1 \phi_2, \tag{20}$$

where $\phi_1 = n_1 v_1$ and $\phi_2 = n_2 v_2$ are, respectively, the volume fractions of solvent molecules and "monomer" segments, with V_m the mixture volume and χ the well-known (Flory) χ-parameter. Clearly, n_1 and n_2 are the solvent and polymer segment number densities, respectively. The corresponding chemical potentials, which are obtained by differentiating F with respect to the number of solvent molecules and monomer segments, are

$$(\mu_1 - \mu_1^0)/(kT) = \ln \phi_1 + \phi_2\left[1 - \frac{1}{N}\frac{v_1}{v_2}\right] + \phi_2^2(\chi - \phi_1\chi_{\phi_2}) \tag{21}$$

and

$$(\mu_2 - \mu_2^0)/(kT) = \frac{v_2}{v_1}\left[\frac{1}{N}\frac{v_1}{v_2}\ln \phi_2 - \phi_1\left(1 - \frac{1}{N}\frac{v_1}{v_2}\right) + \phi_1^2(\chi + \phi_2\chi_{\phi_2})\right], \tag{22}$$

where the subscripts attached to $\chi(\phi_2)$ indicate partial differentiation. Pattanayek and Juvekar [38] show that

$$U(r)/(kT) = \left[\mu_2/(kT) - \frac{v_2}{v_1}\mu_1/(kT) - \frac{1}{N}\ln \phi_2\right]\Bigg|_{\phi_2^\infty}^{\phi_2}, \tag{23}$$

which leads to

$$U(r)/(kT) = \frac{v_2}{v_1}[-\ln(1-\phi_2) + \chi(1-2\phi_2) + (1-\phi_2)\phi_2\chi_{\phi_2}]\Big|_{\phi_2^\infty}^{\phi_2}. \tag{24}$$

Note that $\phi_2+\phi_1=1$ and $\phi=nl^3$ so $\phi_2=\phi v_2/l^3$. Equation (23) expresses the self-consistent mean-field potential for the inhomogeneous polymer layer in terms of data for homogeneous (semidilute) polymer solutions. The ratio v_2/v_1 that multiplies the chemical potential of the solvent gives the number of solvent molecules displaced by a single polymer segment. Therefore, U can be interpreted as a free energy cost to transfer a polymer segment from the bulk to the inhomogeneous polymer layer. This free energy excludes the translational entropy of the polymer [third term in Eq. (23)] because this is accounted for by solving Eq. (18).

Pattanayek and Juvekar obtained the coefficients of quadratic polynomials that capture the dependence of χ upon temperature and the polymer segment volume fraction, ϕ_2. The composition dependence of χ is reported to originate from hydrogen bonding between PEG segments and water molecules. This gives rise to both "energetic" and entropic

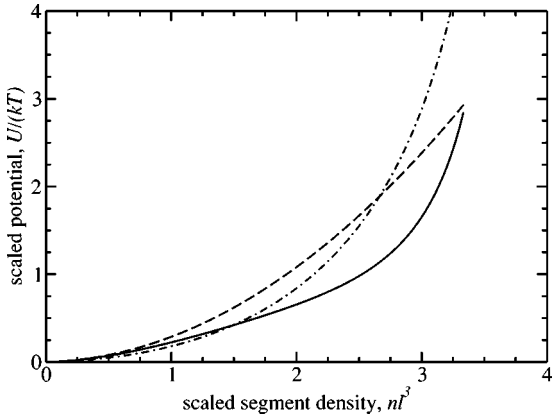

FIG. 1. The scaled self-consistent mean-field potential $U/(kT)$ for aqueous PEO/PEG as a function of the scaled statistical segment density, $\phi = nl^3 = \phi_2 l^3/v_2$, at temperature $T = 25\ ^\circ$C. The solid line is the full expression based on Pattanayek and Juvekar's correlation for $\chi(\phi_2, T)$ [38], the dashed line is an $O(\phi_2)$ accurate expansion of the full expression, and the dash-dotted line is the full expression with $\chi = 0.48$. Other parameters are $v_2/v_1 = 3.3$, $v_2 = 0.27l^3$, $l = 0.71$ nm, and $\phi^\infty = 0$.

contributions to the free energy. The polynomial coefficients[4] were obtained by fitting Flory's model, via Eqs. (21) and (22), to phase-equilibrium data from a variety of sources in the literature (see [38]). Figure 1 shows how $U/(kT)$ depends on ϕ at $T = 25\ ^\circ$C. Note that, while χ is *greater* than 0.5 at infinite dilution ($\phi \to 0$), the expansion of Eq. (24) for small ϕ_2, with $\phi_2^\infty = 0$, is

$$U/(kT) = \frac{v_2}{v_1}\{\phi_2[1 - 2(\chi - \chi_{\phi_2})] + \phi_2^2[1/2 + (3/2)\chi_{\phi_2\phi_2} - 3\chi_{\phi_2}] + O(\phi_2^3)\}, \tag{25}$$

with $\chi \approx 0.644$, $\chi_{\phi_2} \approx 0.163$, and $\chi_{\phi_2\phi_2} \approx 0.702$ evaluated from Pattanayek and Juvekar's polynomials at $\phi_2 = 0$ and $T = 25\ ^\circ$C. At the relatively low monomer densities of interest in this work ($\phi < 0.6$), Fig. 1 shows that Eq. (25) provides an excellent approximation to the full expression (24). Note that the leading-order term in Eq. (25) demonstrates how the *effective* value of χ depends on χ_{ϕ_2}. At $T = 25\ ^\circ$C, for example, its value at infinite dilution is $\chi^* \approx 0.644 - 0.163 = 0.481$, so water is, indeed, a (moderately) "good" solvent for PEG at this temperature, even though $\chi(0) > 0.5$. The scaling theory for brushes pointed to in the introduction gives a nominal segment density $\phi \sim (\sigma l^2)^{3/2 - 1/(2\nu)} \approx 0.17$ with $\sigma l^2 = 0.072$ and $\nu = 3/5$. While the mean-field potential given by Eq. (24) yields a relatively weak, repulsive potential, $U/(kT) \approx 0.025$, it is shown below that brushlike conformations prevail with $\sigma l^2 \approx 0.072$ when $N \geqslant 30$ and, hence, the molecular weight exceeds approximately 1.5 kg mol^{-1}.

The connection between $G(r, r', s)$ and $\phi(r)$ comes from the so-called *composition law* [16,57]

$$\phi(r) = \alpha e^{U(r)/(kT)} \int_0^N \int_a^\infty G(r', a, s) G(r, r', N - s) \mathrm{d}r' \mathrm{d}s, \tag{26}$$

where α is a constant to ensure the correct grafting density. For example, the number of chains grafted per unit area of a spherical substrate with radius a is

$$\sigma = (l^3 a^2 N)^{-1} \int_a^\infty \phi(r) r^2 \mathrm{d}r. \tag{27}$$

The polymer segment density distribution is calculated by solving Eqs. (18), (24), and (26) in a spherical coordinate system with r as the single independent variable. The boundary and "initial" conditions applied in this work are

$$\frac{l}{2}\frac{\partial G}{\partial r} = G \text{ at } r = a \tag{28}$$

and

$$G(r, r', 0) = \delta(r - r'), \tag{29}$$

respectively. More sophisticated boundary conditions, which incorporate an adsorption-energy parameter χ_s and account for inhomogeneity of the surface-interaction region, can be applied [37,38]. For repulsive interactions, however, the segment density distributions are insensitive to such details at distances beyond approximately one segment length from the surface. Equation (28) is a suitable boundary condition for "hard," impenetrable grafting surfaces and is equivalent to setting $G(a - l/2, r', s) = 0$ [35].

The solution of Eq. (18) is calculated using a Crank-Nicholson finite-difference method [58]. Because the self-consistent segment density profile and, hence, the self-consistent potential are initially unknown, an initial "guess" is made, which is then improved upon by iteration. At each iteration, a fraction β of the "new" segment density distribution is added to a fraction $1 - \beta$ of the "old" distribution. The convergence of this procedure depends on β, the initial estimate for $\phi(r)$ or $U(r)/(kT)$, and, of course, the dimensionless parameters χ, N, v_1/v_2, v_2/l^3, σl^2, and a/l that characterize the polymer layers.[5]

III. INTERPRETATION OF COHEN AND KHOROSHEVA'S EXPERIMENTS

In this section, the electrokinetic model is used to interpret Cohen and Khorosheva's experiments reporting the electrophoretic mobility of spherical liposomes with coatings of terminally anchored PEG. The composition of the liposomes was described briefly in the Introduction. Cohen and Khorosheva interpreted their data with a theory they developed for flat surfaces ($\kappa a \gg 1$ and $L \gg a$). Their model invoked the Debye-Hückel approximation[6] and relaxed continuity of the

[4] In a private communication, Professor Juvekar pointed out that the temperature in Table I of Pattanayek and Juvekar's paper [38] should be expressed in °C.

[5] Here, $\sigma = d^{-2}$ is the grafting density, not the dimensionless surface-charge density.

[6] In practice, the Debye-Hückel approximation is reasonable when $|\psi| < 2$.

shear stress and, hence, the velocity gradient at the outer edge of a steplike polymer layer. They clearly acknowledged the limitations of this theory and used it to infer polymer layer thicknesses and (hydrodynamic) permeability from measured electrophoretic mobilities.

A. Cohen and Khorosheva's theory

It remains to establish the conditions under which CK's theory is accurate and, hence, whether it provides a reliable interpretation of the experiments. Before presenting the results of new calculations that solve the full set of electrokinetic transport equations, with a self-consistent mean-field description of the polymer, let us first establish the limitations of CK's model *and* verify the accuracy of the full model.

Figure 2 compares Ohshima's flat-plate ($\kappa a \to \infty$ and $L'/a \to 0$) theory [52] with the full model and CK's simplified theory. The upper and lower subfigures are representative of characteristically thin and thick polymer layers, respectively. The comparison of theory and experiment could certainly be improved at lower ionic strengths by adjusting the surface potential to mimic the effect of charge being displaced behind a shear plane (e.g., [5,7]). However, the primary interest here is to compare the analytical and numerical calculations, so the experimental data are shown for qualitative purposes and to demonstrate that the parameters (see figure caption) are consistent with CK's fit of their model to the data at moderate and high ionic strengths. For clarity, the three theories are presented with the same parameters *and* constant surface charge. Clearly, the deviation of CK's model from Ohshima's flat-plate model and, indeed, the full model, is significant.

The mobility-ionic strength relationship suggested by Ohshima's theory and the full calculations at high ionic strengths suggest that the principle weakness of CK's model arises from the discontinuous change in the hydrodynamic (shear) stresses at the outer edge of the coatings, rather than the finite ratios L'/a and κa. As expected, Ohshima's theory asymptotes to the full electrokinetic model at high ionic strength. While Ohshima's formula for arbitrary surface potentials (dash-dotted lines), given in the form of a series [[52], Eq. (11.4.24)], is slightly closer to the full theory than his simpler expression for low surface potentials (dotted lines) [[52], Eq. (11.4.27)]

$$M = (3|\zeta|/2)[1/\cosh(L'/\ell) - (\kappa\ell)^{-1}\exp(-\kappa L') \times\{1/(\kappa\ell) + \tanh(L'/\ell)\}]/[1 - 1/(\kappa\ell)^2], \qquad (30)$$

the finite particle size and, hence, the effects of polarization are evidently the most limiting aspects of the analytical theory when $\kappa a < 500$.

The qualitative form of the mobility-ionic strength relationship provided by the full model and, indeed, the experiments, suggests that polarization plays a significant role in decreasing the mobility of liposomes with low-molecular-weight coatings (upper subfigure, Fig. 2) at low ionic strength. With thicker layers (lower subfigure, Fig. 2), polarization is attenuated because the polymer diminishes the convective contribution to the ion flux, thereby increasing the effectiveness of molecular diffusion in restoring the equilibrium state of the diffuse double layer.

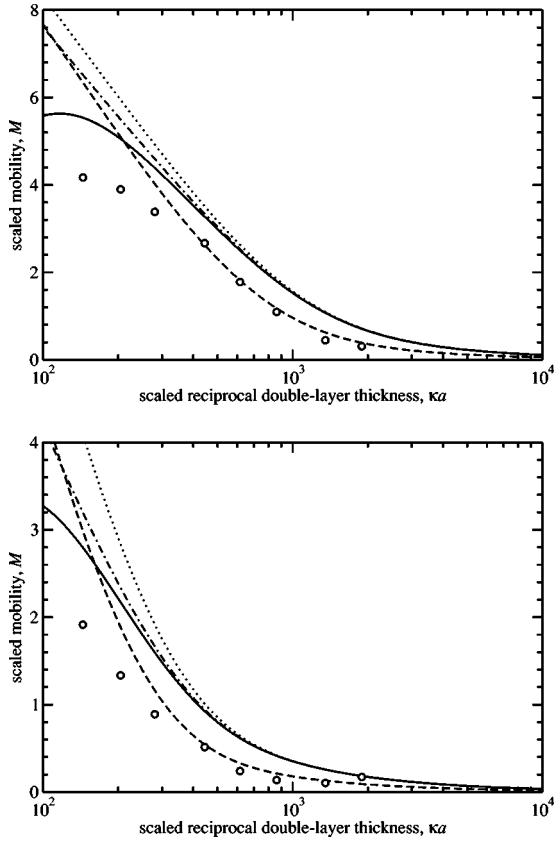

FIG. 2. The (scaled) electrophoretic mobility $M = 3\eta eV/(2\epsilon_s\epsilon_0 kTE)$ of spherical liposomes with coatings of terminally anchored PEG as a function of the (scaled) reciprocal double-layer thickness κa (aqueous NaCl at $T = 25\,^{\circ}\mathrm{C}$). The molecular weights of the PEG are $M = 1$ (*top*) and 5 kg mol^{-1} (*bottom*), with a particle radius $a = 1.75\ \mu$m and (constant) surface charge density $\sigma = -1.95\ \mu\mathrm{C\ cm^{-2}}$. The dashed lines are Cohen and Khorosheva's simplified theory [7] with parameters fitted to their experimental data (circles): $L' = 2.6$ nm and $\ell = 1.6$ nm (*top*); $L' = 13.2$ nm and $\ell = 4.7$ nm (*bottom*). The solid lines interpolate numerically exact solutions of the full electrokinetic model with steplike segment density profiles ($\delta/L = 10^{-3}$) [6] (symbols discarded for clarity) and Cohen and Khorosheva's estimates of L' and ℓ. The dotted and dash-dotted lines are Ohshima's analytical theory (see text) for the flat-plate limit in which $L/a \to 0$ and $\kappa a \to \infty$ [52].

Note that the segment density distributions adopted in full model (Figs. 2 and 3) were specified with a complementary error function, which approaches the step functions in the analytical theories as the characteristic width of the coating edge δ vanishes. The results in Fig. 2, with $\delta/L' = 10^{-3}$, demonstrate that the numerical approach furnishes accurate solutions of the governing equations, even when there are large disparities in the length scales a, κ^{-1}, L', and δ.

B. Specification of the model parameters

The dimensional parameters that characterize CK's experiments are listed in Table I. While many of these, such as the ionic strength, are relatively straightforward to measure

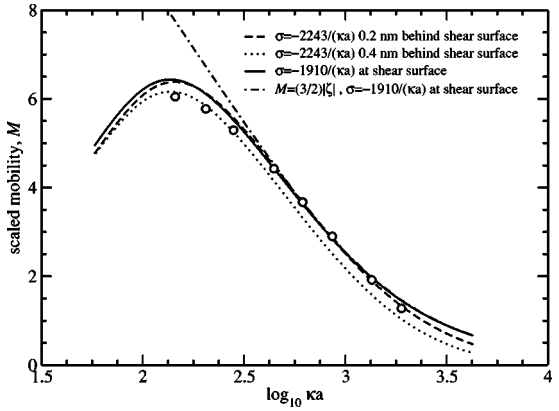

FIG. 3. The (scaled) electrophoretic mobility $M=3\eta eV/(2\epsilon_s\epsilon_0 kTE)$ of bare spherical liposomes as a function of the (scaled) reciprocal double-layer thickness κa (aqueous NaCl at $T=25\,^{\circ}\mathrm{C}$ with radius $a=1.75\ \mu$m). The solid line is the standard electrokinetic model with a (constant) surface charge density $\sigma\approx-1.95\ \mu\mathrm{C\ cm^{-2}}$ residing at the shear plane ($r=a$). The dashed and dotted lines are from calculations with a surface charge density $\sigma\approx-2.29\ \mu\mathrm{C\ cm^{-2}}$ (corresponding to the "actual" surface charge) residing 2 and 4 Å, respectively, *behind* the shear plane. Symbols are experimental data of Cohen and Khorosheva [7]. Neglect of surface curvature at low ionic strength is emphasized by Smoluchowski's well-known theory $M=(3/2)|\zeta|$ with $\sigma\approx-1.95\ \mu\mathrm{C\ cm^{-2}}$ *at* the shear plane (dash-dotted line).

and, hence, can be treated as "known," many are not. These include, for example, the surface charge density, the polymer grafting density, and various statistical characteristics of the polymer chains—namely, the number N, length l, and volumes v_1 and v_2 of the statistical segments and solvent molecules, respectively.

1. Liposome size

The diameters of the liposomes used in CK's experiments were in the range $2-5\ \mu$m. The particle size does not appear in their theory, because κa is assumed large enough for the mobility to be independent of the radius. However, the particle size is relevant at low ionic strengths, when the double layer is not infinitesimally thin compared to the particle radius. The particle radius adopted for the calculations in this work is $a=1.75\ \mu$m. However, given the logarithmic scale over which the double-layer thickness varies with ionic strength ($I=0.5-100$ mM), it is unlikely that small relative changes in the particle radius could significantly affect the results.

2. PEG grafting density

Cohen and Khorosheva estimate the average distance between the grafted chains to be $d\approx26$ Å, which corresponds to an average surface area, per chain, of approximately 700 $\mathrm{Å}^2$ or $O(10^6)$ chains per liposome. This value can be inferred from the reported 1:9 ratio of PEG-PE to PC lipids used to synthesize the liposomes and the known surface area per lipid ($\approx70\ \mathrm{Å}^2$). Clearly, the PEG-derivatized lipids must be assumed to be uniformly distributed both within and among all the liposomes.

3. Liposome surface charge density

The surface potential can be inferred from the electrophoretic mobilities of the bare liposomes using the well-

TABLE I. Dimensional parameters used to interpret Cohen and Khorosheva's [7] measurements of the electrophoretic mobility of liposomes with terminally anchored PEG coatings. See text for details.

Surface charge density[a]	σ	$-1.95\ \mu\mathrm{C\ cm^{-2}}$
Particle radius	a	$1.75\ \mu$m
Solvent dielectric constant	ϵ_s	78.5
Solvent viscosity	η	8.90×10^{-4} kg (ms)$^{-1}$
Solvent density	ρ_s	997 kg m^{-3}
Temperature	T	298 K
Ionic strength	I	$10^{-4}-0.56$ M
Na^+ limiting conductivity	Λ_1	50.1 Sc m^2 mol^{-1}
Cl^- limiting conductivity	Λ_2	76.4 Sc m^2 mol^{-1}
Monomer molar mass	M_m	44 g mol^{-1}
Number of statistical segments per chain	N	$0.62(10^3M-32)/44$
PEG molar mass	M	0, 0.35, 1, 2, 3, 5 kg mol^{-1}
Statistical-segment length	ℓ	0.71 nm
Monomer-segment length	ℓ_m	0.44 nm
Statistical-segment volume	v_2	$0.27\ell^3$
Solvent-molecule volume	v_1	$0.082\ell^3$
Grafting density	$\sigma=d^{-2}$	$(0.268/\ell)^2$
Statistical-segment hydrodynamic radius[b]	a_s	0.175 Å

[a]From the bare liposome mobility (at high ionic strength) and application of the *standard* electrokinetic model with the shear surface at $r=a$.
[b]Fit of the full electrokinetic model with a self-consistent mean-field description of the polymer.

known *standard* electrokinetic model [48], which, for large κa *and* low surface potential, $|\zeta|$, is accurately approximated by Smoluchowski's formula $M=(3/2)|\zeta|$. Numerical solutions of the full electrokinetic model for bare liposomes[7] show that the assumption of a constant surface charge is reasonable when the concentration of added salt (NaCl) is greater than approximately 6 mM (see Fig. 3). The calculations were performed with $\sigma \approx -1.95\ \mu\mathrm{C\ cm^{-2}}$, which is equivalent to an average surface area, per elementary, univalent surface charge, of approximately 28.6^2 Å^2 *at* the *shear plane*.[8]

The surface charge adopted in this work is, strictly speaking, an *effective value*. The charge inferred by the electrophoretic mobility of many colloids tends to be lower than the *actual* charge because the charge resides behind a *shear plane*, i.e., a surface beneath which the fluid is immobile. If the charge is independent of the concentration of ions in the surrounding electrolyte, then the potential *at* the shear plane, $|\zeta|$, necessarily decreases with increasing ionic strength. Figure 3 shows that there exists no significant difference between the mobility of bare liposomes with the actual charge *behind* a shear plane and a diminished effective charge *at* the shear plane. Indeed, an effective charge density of $\sigma \approx -1.95\ \mu\mathrm{C\ cm^{-2}}$ at the shear plane (solid line) yields mobilities very close to those with $\sigma \approx -2.29\ \mu\mathrm{C\ cm^{-2}}$ located 2 Å (dashed line) and 4 Å (dotted line) behind the shear plane. Recall, a charge density of $-2.29\ \mu\mathrm{C\ cm^{-2}}$ reflects the stoichiometric ratio of charged to uncharged lipids (1:9) and the average surface area per lipid.

The concave-down shape of the mobility-ionic strength relationship is indicative of double-layer polarization. The departure of Smoluchowski's mobility formula from the "exact" calculations for bare liposomes (Figs. 3 and 5) demonstrates that the diffuse double layer is not infinitesimally thin compared to the particle radius. Furthermore, the departure of the exact calculations from the experiments indicates that the *effective* surface charge varies with ionic strength. When the surface potential is sufficiently high and the double layer sufficiently thick, the mobility *may* decrease with increasing charge because of polarization and the resulting *mobility maximum* [48]. Nevertheless, with the prevailing values of $|\zeta|$ and κa, the mobility should increase with the surface charge.

If the decrease in effective charge were attributed entirely to an outward displacement of the shear plane, then there remains the question as to how and why the displacement varies with the bulk ionic strength. The results in Fig. 3 with charge residing behind a shear plane indicate that the distance between the shear and charged surfaces increases from approximately 2 to 4Å. Because the difference between theory and experiment is small compared to the influence of the polymer, the role of counterion binding or *charge regulation* is not addressed here [see [59]].

The charged lipids may migrate under the influence of the applied electric field. Such reorganization has been observed on macroscopically flat supported lipid bilayers [60,61]. For liposomes, migration would increase the induced dipole, and it is well known that such polarization decreases the electrophoretic mobility, thereby decreasing the surface charge inferred from a model that assumes immobile charge. Such a redistribution cannot affect the mobility to linear order in the applied electric field strength, however, because the perturbed charge distribution modifies the (surface) boundary condition for the electrostatic potential, and such perturbations do not affect the electrophoretic mobility [48]. An unambiguous test for the significance of this nonlinearity would be to report the mobility, particularly at low ionic strengths, at several electric field strengths. If charge migration is significant, then the mobility would decrease with increasing field strength.

4. Statistical PEG segment length and volume

The statistical characteristics of the polymer chains, as specified by the number of segments per chain, and the length and volume of the segments, are not straightforward to determine. However, they can be inferred from studies of dilute aqueous solutions of PEO. Devanand and Selser [62] measured the radius of gyration of relatively long PEO chains in dilute aqueous solution, with molecular weights in the range 10^2–10^3 kg mol^{-1}. Their light-scattering experiments yield a radius of gyration that scales according to classical theoretical predictions for flexible chains in a *good* solvent, $R_g = 0.215 M^{0.583\pm0.031}$ Å at 30 °C, with M the molecular weight (g mol^{-1}). Unfortunately, there does not exist a tractable theory that permits l and N to be inferred from these data. Rather, the parameters must be obtained under *theta* conditions, when repulsive excluded-volume interactions are balanced by attractive dispersion forces.

The number of statistical segments, N, and the corresponding statistical-segment length l were obtained from a correlation for the radius of gyration of PEO chains under *theta* conditions $R_g = a_m M^{1/2}$, with M the molecular weight (g mol^{-1}) and $a_m = 0.343$ Å (e.g., [63]). Since the radius of gyration of an ideal chain (real chain in a *theta* solvent) is well known to be $R_g = l(N/6)^{1/2}$, the length of a *monomer* segment is $l_m \approx 0.44$ nm [31,64], and $Nl = (M/M_m) l_m$ with $M_m \approx 44$ g mol^{-1} the molecular weight of a PEG/PEO monomer, the Kuhn length is $l = 6 M_m a_m^2 / l_m \approx 0.71$ nm. It follows that $N \approx 0.623 M/M_m$, from which it is evident that each statistical segment comprises approximately 1.6 PEG monomers.

As described in Sec. II C, given N and l for chains with a known molecular weight, the self-consistent-field model requires knowledge of v_2/v_1, v_2/l^3 and $\chi(\phi_2)$. The calculations in this work were performed using the empirical correlations of Pattanayek and Juvekar [38]. They calculated the molar volume of a PEO statistical segment from the density of aqueous PEO solutions as measured by Hasse and coworkers [65]. At $T = 25$ °C, their correlations give $v_2 = 4.61^3$ Å$^3 \approx 0.27 l^3$ with $l = 0.71$ nm. As expected from Devanad and Selser's light-scattering measurements [62], Pattanayek and Juvekar's analysis of thermodynamic data, as presented in Fig. 1, for example, confirms that water is indeed a good solvent for PEO/PEG at room temperature.

[7] Solutions of the standard electrokinetic model are calculated by setting the polymer segment density to zero.

[8] The dimensionless surface charge density is $\sigma = -\partial\psi(r=\kappa a)/\partial r \approx -1910/(\kappa a)$.

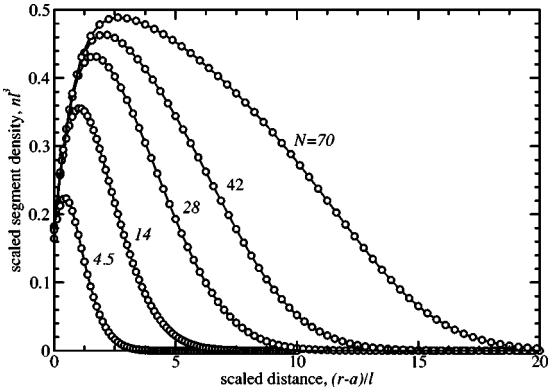

FIG. 4. The radial segment density distribution $\phi = nl^3$ of PEG chains terminally anchored to the surface of spherical liposomes with radius $a = 1.75$ μm as a function of the (scaled) distance from the surface of the bare liposome surface, $(r-a)/l$. The circles (interpolated with solid lines) are calculations for various numbers of statistical segments per chain, $N = 4.5$, 14, 28, 42, and 70, with $v_2/v_1 = 3.3$, $v_2/l^3 = 0.27$, $\sigma l^2 = 0.072$, and $l = 0.71$ nm. The self-consistent mean-field potential is specified according to Eq. (24).

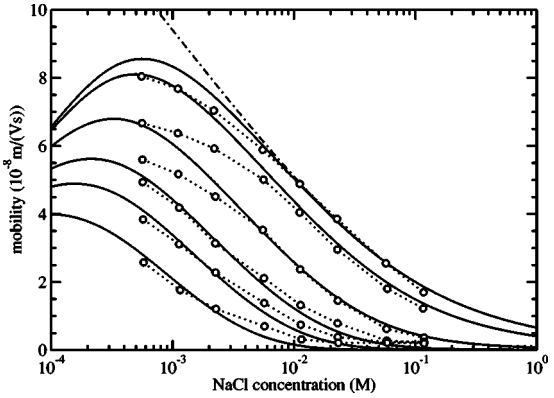

FIG. 5. The electrophoretic mobility V/E of spherical liposomes with coatings of terminally anchored PEG as a function of the bulk ionic strength for various numbers of statistical segments per PEG chain, $N = 0$ (bare liposome), 4.5, 14, 28, 42, and 70 (increasing downward); the molecular weights of the PEG chains are $M = 0$, 0.35, 1, 2, 3, and 5 kg mol^{-1}, respectively. The solid lines interpolate numerically exact solutions of the full electrokinetic model with a self-consistent mean-field description of the polymer segment density distributions (symbols omitted for clarity). The circles (with dotted lines to guide the eye) are Cohen and Khorosheva's experimental data [7], and the dash-dotted line is Smoluchowski's well-known theory for a bare particle with *constant* surface charge, $M = (3/2)|\zeta|$. See Table I for parameters.

A statistical segment length of 3.5 Å has often been adopted for PEG in the biophysics literature (e.g., [5,7,31,66,67]). It is unknown to the author from where this value originated and, indeed, what accuracy is to be inferred. In some cases, it has been used to characterize the monomer length. It is often referred to as an approximate value and is clearly inconsistent with the arguments above, which suggest a value approximately twice as large. In support of the value adopted in this work and by Pattanayek and Juvekar is Russel and co-workers' survey of data in Ref. [68] giving $l_m = 0.44$ nm and $l = 0.60$ nm ([35], Table 6.1). The value of 3.5 Å has been associated with the Flory radius expressed as $R_F = 3.5N_m^{3/5}$ Å, with N_m the number of monomers per chain. It is therefore tempting to compare this with Devanad and Selser's [62] correlation, $R_g = 0.215M^{0.583\pm0.031}$ Å. Substituting $M = 44N_m$ g mol^{-1} gives $R_g = 1.95N_m^{0.583}$ Å, so if R_F is associated with the mean-squared end-to-end distance R and we apply the ratio $R = \sqrt{6}R_g$ for ideal chains, there results $R_F = 4.8N_m^{0.583}$ Å, which is somewhat closer to the indicated $R_F = 3.5N_m^{3/5}$ Å.

C. Segment density distributions

Segment density distributions are shown in Fig. 4 for the five molecular weights of PEG used in CK's experiments. From the scaling theory pointed to in the Introduction, a transition from mushroom conformations to brushlike structure is expected when $d \sim lN^{\nu}$. With $\sigma l^2 = 0.072$ and $\nu = 3/5$, for example, the transition should occur when $N \sim 10$, so the lowest molecular weight PEG with $N = 4.5$ and, possibly, the next shortest chains with $N = 14$ should adopt Gaussian-like distributions with a nominal coating thickness $L' \sim lN^{3/5}$ and segment density $\phi \sim 0.072N^{2/5}$. The longer chains, with $N = 28$, 42, and 70, should adopt bushlike conformations with $L' \sim 0.42lN$ and $\phi \sim 0.17$.

Indeed, the transition from mushroomlike to brushlike structure is evident when the segment density distributions are plotted with the axes scaled appropriately. For clarity, the data in Figure 4 are plotted without such scaling. Nevertheless, it is clear that the coatings suggested by scaling theory to be brush like are, perhaps, much less homogeneous than one might otherwise expect. With $N = 70$, the profile exhibits the characteristics of a *parabolic* brush [17]. For these relatively low-molecular-weight polymers, brushlike characteristics manifest much more distinctly in the scaling of the averaged segment density and hydrodynamic coating thickness. These are examined in detail below, after the hydrodynamic radius of the segments is established via the electrophoretic mobility. Further details of the coating structure, including the distribution of end-segments, can be obtained from the self-consistent mean-field calculations. These are discussed in the references pointed to in the Introduction.

D. Electrophoretic mobility

The hydrodynamic radius of the polymer segments, a_s, is adopted in this work as the primary "fitting" parameter. Unlike the coating thickness and permeability, a_s is assumed not to vary with the polymer chain length. Instead, it is taken to be an intrinsic characteristic of the monomer, similarly to the molar volume v_2 and the statistical segment length l. The electrophoretic mobilities shown in Fig. 5 were calculated from the HSR electrokinetic model using the polymer segment density distributions shown in Fig. 4. With $a_s = 0.175$ Å, the full model provides an excellent "fit" to CK's experimental data over a wide range of ionic strengths and PEG chain lengths.

The most significant difference between theory (solid curves) and experiment (circles) occurs at the lowest ionic

strengths, for particles with the two thinnest layers and, possibly, the bare liposomes. It is possible to improve the fit by allowing the effective surface charge to vary with the bulk ionic strength, as demonstrated in Fig. 3 for bare liposomes. Such an adjustment does not account for the influence of low-molecular-weight polymer at low ionic strengths, however. The discrepancy might be attributed to lateral mobility of surface charges and polymer, which is clearly not accounted for in the present model. Recall, in CK's experiments, the charged lipids, which bear the surface charge, also anchor the polymer. Therefore, it is not unreasonable to expect surface mobility to decrease with increasing molecular weight, vanishing when $d < lN^{\nu}$. Furthermore, one should expect the mobility of charged PEG-derivatized lipids to have a similar (qualitative) dependence on the bulk ionic strength as the liposome itself. Clearly, the comparison of experiment and theory suggests that surface-charge mobility decreases the particle mobility. This may be attributed to polarization of the surface charge layer, and such a redistribution of charge would manifest in a (scaled) particle mobility that depends on the applied electric-field strength [48].

Explanations based on shape fluctuations are difficult to justify because these liposomes are multilamellar and, presumably, much more rigid than unilamellar vesicles (see [69]). Furthermore, the electrophoretic mobility at values of κa where Smoluchowski's theory is valid is well known to be independent of particle size and shape. At present, the influence of a nonuniform distribution of polymer and charge throughout the lamellae is uncertain. Theoretical steps toward understanding the distribution and influence of PEG-lipids on curved bilayer membranes have been taken by Rovira-Bru *et al.* [70]; it is not clear that these results can be applied to large multilamellar liposomes, however. Finally, it should be noted that the influence of polymer on the effective dielectric constant in the layers has been neglected entirely. The polymer presumably lowers the effective dielectric constant, thereby increasing correlations between ions in the electrolyte and on the underlying surface. Given the low polymer volume fractions $n v_2 = \phi v_2 / l^3 < 0.15$, it is difficult at present to quantify this influence and, indeed, to distinguish it from the (dominant) hydrodynamic one.

E. Coating thicknesses, densities, and permeabilities

The *effective* coating thickness reflects polymer and electroviscous drag when the particle is under translation in the absence of an applied electric field. An increase in the effective size with decreasing ionic strength arises from electroosmotic flow that resists deformation of the equilibrium double layer. In Fig. 6, the electroviscous effect is clearly evident at low ionic strengths for particles with low-molecular-weight polymer coatings. Increasing the double-layer thickness, by decreasing the bulk ionic strength, increases the characteristic ion diffusion time, and this increases the effectiveness of convection in polarizing the double layer. Also, the high surface potentials that prevail at low ionic strengths support a significant charge density, which, in turn, contributes to the electrical body force on the fluid inside the double layer. Clearly, polymer slows the convective flow and, hence, attenuates double-layer polarization. Moreover, the electroviscous contribution to the effective particle size diminishes with increasing layer thickness. Therefore, at high ionic strengths, polarization is negligible and the *effective* coating thickness approaches the *hydrodynamic* thickness.

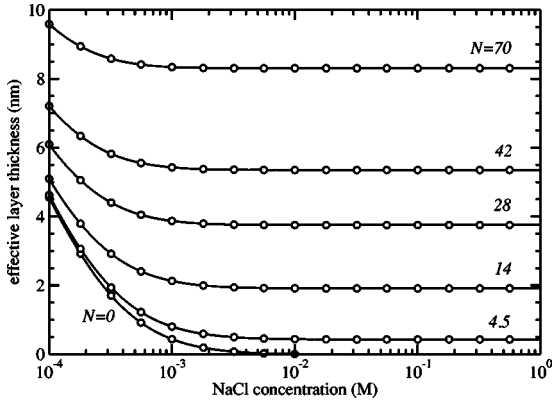

FIG. 6. The *effective* thickness L of coatings of PEG terminally anchored to spherical liposomes with radius $a = 1.75$ μm as a function of the bulk ionic strength. The circles (interpolated with solid lines) are from theoretical calculations with $N = 4.5$, 14, 28, 42, and 70 statistical segments per chain. See Table I for parameters.

As shown in Fig. 7, the hydrodynamic coating thickness increases as $L \approx 0.22Nl$ when $N > 30$. The thickness of the lower-molecular-weight PEG coatings is significantly smaller than expected from the segment density distributions shown in Fig. 4. These layers are much more permeable than their higher-molecular-weight counterparts. According to the present mean-field theory, the segment density distribution is not representative of a single PEG coil, but rather an average over the relatively dense coils and intervening void space. The accuracy of these calculations clearly depends on whether the mean-field approximations, for the polymer conformation *and* hydrodynamics, are reasonable. The compari-

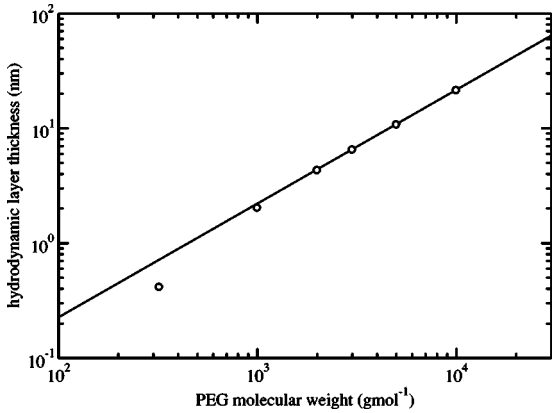

FIG. 7. The *hydrodynamic* thickness L of coatings of PEG terminally anchored to spherical liposomes with radius $a = 1.75$ μm as a function of the PEG molecular mass. The circles are from theoretical calculations with $N = 4.5$, 14, 28, 42, 70, and 140 statistical segments per chain, and the line is a power-law fit $L \approx 0.97 N_m^{0.98}$ Å, with $N_m = M/M_m$ the number of monomers per chain. See Table I for parameters.

TABLE II. Quantitative interpretation of Cohen and Khorosheva's experiments by (i) their simplified analytical theory (CK) and (i) the full electrokinetic model with a self-consistent mean-field description of the PEG segment density distribution (SCMF).

			CK[a]				SCMF (a_s=0.175 Å)		
M (g mol^{-1})	M/M_m	N	L' (nm)	ϕ[b]	ℓ (nm)	a_s[c] (Å)	L[d] (nm)	$\langle\phi\rangle$[e]	$\langle\ell\rangle$[f] (nm)
350	7	4.5	(2.9)	-	-	-	0.42	0.55	1.4
1000	22	14	(2.6)	(0.28)	(1.6)	(0.27)	2.0	0.36	1.7
2000	45	28	4.5	0.32	1.9	0.17	4.3	0.33	1.8
3000	67	42	7.3	0.29	2.9	0.077	6.5	0.33	1.8
5000	113	70	13.2	0.27	4.7	0.032	11	0.32	1.8

[a]CK caution that their theoretical interpretation is not reliable for M=350 and 1000 g mol^{-1} (reported here in parentheses).
[b]Based on a uniform distribution of segments between $r=a$ and $a+L'$, with l=0.71 nm.
[c]Calculated from $a_s=l^3/(6\pi\phi\ell^2)$.
[d]The effective coating thickness at high ionic strength, i.e., in absence of electroviscous effects.
[e]Based on a uniform distribution of segments between $r=a$ and $a+L'$.
[f]Based on a uniform distribution of segments between $r=a$ and $a+L$, with a_s=0.175 Å.

son of theory and experiment rests on the electrophoretic mobilities presented in Fig. 5. It is therefore helpful to compare the results with those inferred from other simpler theoretical interpretations of experiment.

Cohen and Khorosheva's model suggests that each monomer contributes 0.128 nm to the (actual) coating thickness. In the high-molecular-weight limit, their theory leads to coatings approximately 30% thicker than suggested by the full model. At lower molecular weights, but still in the brush regime, their coating thicknesses are in reasonable agreement with the full model. However, the permeabilities and Stokes radii vary considerably, which is clearly inconsistent with expectations for brushes.

Janzen and co-workers [5] inferred a layer thickness of 3 nm for PEG coatings with a molecular weight of 1 kg mol^{-1} ($N\approx 14$) with a grafting density $\sigma l^2\approx 0.072$. Note that the hydrodynamic layer thickness from the full model is 2 nm, with chains extending as far as $5l\approx 3.6$ nm from the grafting surface (see Fig. 4). Clearly, it is difficult to compare uniform, steplike layers with more realistic, nonuniform layers. Neither Janzen *et al.* nor CK reported hydrodynamic layer thicknesses.

Recall, if the polymer segments are modeled as spherical Stokes resistance centers, then the Brinkman screening length is $\ell=(F_s 6\pi a_s n)^{-1/2}$, with the drag coefficient $F_s\approx 1$ when $\phi_s=n(4/3)\pi a_s^3\ll 1$. If the segment density distribution is assumed uniform, then the nominal coating thickness and segment density are related by the "known" grafting density and polymer molecular weight. We may therefore infer from CK's coating thicknesses L' and Brinkman screening lengths ℓ, an average (scaled) segment density $\phi=nl^3$ and hydrodynamic segment radius a_s. These are listed in columns 4–7 of Table II. The nominal (scaled) segment density in column 5 was calculated from CK's values of L' using the values of N (column 3) and l=0.71 nm adopted for the self-consistent mean-field calculations. Because CK's analysis yields coating thicknesses that are close to those obtained from the full model, the resulting segment densities are comparable. However, the permeabilities vary considerably, yielding particularly large values of ℓ for the two coatings with the highest molecular weight polymer. Of course, the corresponding values of a_s to be inferred from CK's data also vary considerably with N. When compared to the full model, it appears that CK's overestimate of L' has been compensated for, in part, by an underestimate of a_s. Indeed, the values of a_s inferred from CK's analysis are very small.

Because the coatings from the self-consistent mean-field calculations are inhomogeneous, the segment densities reported in column 9 of Table II are average values $\langle\phi\rangle$ obtained by dividing the number of segments $4\pi a^2\sigma N$, by the volume enclosed by the underlying bare liposome and a concentric sphere with a radius equal to the *hydrodynamic* radius $(4/3)\pi a^3[(1+L/a)^3-1]$. The Brinkman screening length reported in column 10 is based on this average segment density, i.e., $\langle\ell\rangle\approx(6\pi a_s\langle\phi\rangle/l^3)^{-1/2}$. Of course, in the full model, ℓ varies (radially) with the segment density.

As expected, $\langle\phi\rangle$ and $\langle\ell\rangle$ are independent of N when $N>14$. The transition from mushroomlike to brushlike structure suggested here is consistent with the region over which L increases linearly with N in Fig. 7. For the thinnest coating, $\langle\phi\rangle$ is unrealistically high and, hence, the corresponding value of $\langle\ell\rangle$ is unrealistically low. This is because the hydrodynamic thickness is much smaller than the characteristic width of the segment density distribution $L'\sim lN^{\nu}$, as can be verified by identifying L on the abscissa in Fig. 4.

IV. HYDRODYNAMIC (STOKES) RADIUS OF A STATISTICAL SEGMENT

Recall, the statistical segment length for PEO/PEG in this work is l=7.1 Å, and the length of a C-C bond is 1.54 Å. Clearly, the hydrodynamic radius of the statistical segments, $a_s\approx 0.175$ Å, is remarkably small. While a clear quantitative explanation is elusive, the result is consistent with other

TABLE III. Representative characteristics of polymer layers from electrokinetic studies. The hydrodynamic radius of the segments, a_s, applies to either monomer segments or statistical segments, depending on the assignment of a value to M/M_m or N in columns 3 and 4, respectively. The segment density n is consistent with the assignment of a_s to monomer or statistical segments.

Polymer	M (g mol^{-1})	M/M_m	N	d (Å)	L' (Å)	n (M)	ℓ (Å)	a_s (Å)	$\phi_s=n(4/3)\pi a_s^3$	Ref.
PEG	1000[a]	22	-	26.5	26	2.0	16	0.17	2×10^{-5}	CK [7]
PEG	1000	-	14	26.5	26	1.3	16	0.27	6×10^{-5}	CK [7]
PEG	1000	-	14	26.5	20[b]	1.7	17	0.18	2×10^{-5}	This work
PEG	1000	22	-	26.5	30	1.7	4.9	2.2	0.04	Janzen *et al.* [5]
glycocalyx	-	-	-	-	75	0.072	13	7.0	0.06	Levine *et al.* [2]

[a]CK caution that parameters inferred by their model for this molecular weight may not be as accurate as for the higher molecular weights (see Table II); nevertheless, this choice facilitates a comparison here with the parameters of Janzen *et al.* (line 4).
[b]Hydrodynamic thickness L.

independent applications of the Debye-Brinkman theory. Because the Brinkman permeability is usually adopted as the primary fitting parameter, the Stokes radius must be inferred from previously reported permeabilities and segment densities.

Table III summarizes characteristics of polymer layers from studies where electrokinetic theory has been used to interpret experimental data. The hydrodynamic radius of a PEG segment from CK's study was obtained from their reported values of ℓ and the segment density based on the number of segments per chain N, the coating thickness L', and the grafting density d^{-2}. The resulting hydrodynamic radii, for either monomer segments (line 1) or statistical segments (line 2), are comparable to the value obtained from the full model (line 3). Recall, in CK's study, both ℓ and L' were adopted as fitting parameters. In striking contrast are the hydrodynamic radii of the segments adopted in the other two studies (lines 4 and 5) for PEG and glycocalyx layers. These authors specified the hydrodynamic size of the segments and adopted the coating thickness as a fitting parameter. Clearly, the different methodologies, applied with theoretical models that are fundamentally similar, lead to different interpretations of experiment.

Let us briefly examine the (incorrect) notion that the anomalous hydrodynamic radius is an artifact of the spherical approximation of the polymer segments. Given that the drag force on a slender ($l_c \gg a_c$) rod with length $2l_c$ and radius a_c is $f_\parallel=4\pi\eta l_c V/\ln(l_c/a_c)$ and $f_\perp=8\pi\eta l_c V/\ln(l_c/a_c)$ when the flow is parallel and perpendicular to the director, respectively, equating an *average* force on a rod $(f_\parallel+f_\perp)/2$ to the average force on a sphere $6\pi\eta a_s V$, gives

$$a_s = l_c/\ln(l_c/a_c). \tag{31}$$

Clearly, in the absence of hydrodynamic interactions, a_s should be less than, but of a comparable magnitude to, l_c. If, for example, $2l_c=l=7.1$ Å and $a_c=1.54$ Å, then $a_s=4.3$ Å, so the value of $a_s\approx0.175$ Å inferred from the electrokinetic model and experiments is clearly at odds with this simple analysis.

Cohen Stuart *et al.* [39] compared measured hydrodynamic thicknesses of adsorbed PEO layers with theory, with the polymer segment density specified using the well-known Scheutjens-Fleer lattice theory and (as in this work) a Debye-Brinkman description of the flow. They adopted a semiempirical relationship for the Brinkman screening length, $\ell^2=ca^2(\phi_i^{-1}-1)$, where ϕ_i is the polymer volume fraction in the ith layer of the lattice and a is the so-called elementary layer thickness. For PEO and, hence, PEG, they reported $ca^2=0.5(1.0\ \text{nm})^2=0.5\ \text{nm}^2$ and pointed out that setting the monomer length to $l_m=a/2$ (two monomers per lattice) with $a=1.1$ nm allowed theoretical calculations and experimental data to be superposed. In this work, the statistical segment volume is $v_2\approx0.27l^3$, so ϕ_i in the lattice theory is equivalent to $nv_2=0.27nl^3$. Therefore, equating $\ell^2=ca^2/\phi_i$ to $1/(6\pi a_s n)$, as $\phi_i\to0$, yields $a_s=\phi_i/(6\pi nca^2)\approx0.103$ Å, which is clearly very small. Alternatively, if ϕ_i is interpreted as being equal to $n_m l_m^3$, with n_m and l_m, respectively, the (number) density and length of the monomer segments, then $\ell^2=ca^2/[n_m(a/2)^3]$. In this work, $n=n_m l_m/l=n_m 4.4/7.1$, so $a_s=n_m(a/2)^3/[6\pi n_m(l_m/l)ca^2]\approx0.235$ Å, which is also very small.

Further independent justification for a small Stokes radius comes from Mijnlieff and Wiegel [71], who applied the Debye-Brinkman model, with a Gaussian distribution of polymer segments, to calculate the sedimentation velocity and intrinsic viscosity for dilute poly(α-methyl styrene) (PAMS) in cyclohexane. With a molecular weight of 2000 kg mol^{-1}, for example, the (measured) radius of gyration is $R_g\approx39.5$ nm under *theta* conditions. Assuming a Gaussian distribution of segments, they calculated the concentration of polymer at the "center" of the coils to be $c\approx0.0179$ g cm^{-3}, with a Brinkman screening length there of $\ell\approx9.43$ nm. It follows that the monomer (number) density is $n_m\approx0.15$ M ($M_m\approx118$ g mol^{-1}) and, hence, that the Stokes radius of a monomer ($l_m\approx2.5$ Å) is $a_m=0.065$ Å; the equivalent Stokes radius of a statistical segment with Kuhn length $l=2.21$ nm is $a_s=0.575$ Å. Note that the ratio $a_s/l\approx0.026$ for PAMS is very close to the value established in this work for PEO/PEG, $a_s/l\approx0.025$; it is not unreasonable to expect such a proportionality based on simple hydrodynamic considerations. Once again, the hydrodynamic size of the segments is very small.

In the polymer-physics literature, the Stokes radius is "hidden" in the *hydrodynamic permeability* (e.g., Debye-Beuche [43] or the *draining parameter* in the well-known Kirkwood-Riseman theory (see [72]). For polymer coils, intense fluctuations in the segment density, and the long-range nature of intramolecular hydrodynamic interactions may be invoked to justify shortcomings of Debye-Brinkman theory. It is not clear that such limitations apply to polymer brushes, however. Indeed, mean-field descriptions of the equilibrium structure of polymer layers are supported by experiments that resolve the spatial inhomogeneity. This suggests that the apparent shortcoming arises from the Debye-Brinkman model and, in particular, its neglect of correlations between (microscale) fluctuations in the segment density and fluid velocity. Arguments based on a breakdown of continuum hydrodynamics at small (atomic) scales are unlikely to resolve matters, since the hydrodynamic radii of ions and other small molecules are well known to be comparable to their physical size.

A comprehensive analysis of charged polymer layers is beyond the scope of this work, but it is, nevertheless, interesting to compare predictions of the electrokinetic model with available data for associative diblock copolymers, as reported by Cottet and co-workers [73]. These micellular particles comprise a small, impermeable hydrophobic core with a thick and permeable charged layer. When Donnan equilibrium prevails inside the charged layer, i.e., at sufficiently high ionic strengths, and with a "corona" that is much thicker than the Brinkman screening length, the full electrokinetic model yields a remarkably simple result: the particle electrophoretic mobility becomes equal to the mobility of a "free" polymer segment, and, furthermore, when the charge density is proportional to the segment density the mobility is independent of the segment density distribution (see [6]). For example, equating the electrical body force $n(r)zeE$, where z is the *effective* valence of a segment, to the Darcy drag force $n(r)6\pi\eta a_s V$, yields a dimensional electrophoretic mobility

$$V/E = ze/(6\pi\eta a_s), \tag{32}$$

which is clearly independent of the segment density distribution. Indeed, the mobilities of poly(styrene sulfonate) copolymer aggregates reported by Cottet *et al.*, with widely varying molecular weight, segment density, and hydrodynamic radius, differ by less than 10% in 40 mM sodium borate electrolyte ($\kappa^{-1} \approx 2$ nm) [73]. Equation (32) and the measured mobility $V/E \approx -35 \times 10^{-9}$ m^2/(V s) give $a_s \approx 2.73|z|$ Å, and Manning's counterion condensation theory [74] limits the effective linear charge density to e/l_B when $\beta/l_m \geq l_B^{-1}$. Here, $l_B = e^2/(4\pi\epsilon_0\epsilon_s kT) \approx 7.1$ Å is the *Bjerrum length* and β is the fraction of charged monomer segments. It follows that $|z| \approx (l_m/l_B)\beta \approx (2.5/7.1)\beta$. Note that counterion condensation reduces the Donnan potential significantly and, moreover, the mobility remains finite with vanishing electrostatic potential. Now, since β is unknown, but is typically in the range 0.8–1.0, the ratio a_s/l is in the range 0.31–0.38. Clearly, in contrast to the neutral polymers above, the effective size of these charged segments is comparable to their physical size [recall Eq. (31)]. Evidently, the microscale hydrodynamics are qualitatively different from those prevailing with neutral polymer. With neutral polymer, the fluid is suggested to preferentially flow through regions of low segment density, thereby (substantially) reducing the average drag force per segment. With charged polymer, however, at sufficiently high ionic strengths and with $\phi = n(4/3)\pi a_s^3 \ll 1$, the forces driving relative motion of the polymer and interstitial electrolyte are relatively insensitive to density fluctuations on both large and small scales.

V. SUMMARY

This work presents the first theoretical predictions of the mobility of spherical, polymer-coated ("soft" or "fuzzy") colloids based on a detailed model of the polymer segment density distribution and numerically exact solutions of the full electrokinetic model. Numerical calculations were used, together with experimental measurements of the electrophoretic mobility of liposomes with terminally anchored PEG [7], to infer a fundamental characteristic of the polymer—the *effective* hydrodynamic size (Stokes radius) of the statistical segments. In principle, the model is now capable of predicting the mobilities and other single-particle characteristics (e.g., diffusion coefficient) of a variety of colloids with terminally anchored PEG coatings, given parameters such as the size of the underlying bare colloid, the surface charge, ionic strength, and the amount and molecular weight of the grafted polymer.

The remarkably small Stokes radius for PEG/PEO segments ($a_s \approx 0.175$ Å with $l \approx 7.1$ Å) is suggested to be an artifact of the mean-field (Debye-Brinkman) description of the interstitial flow, and it was demonstrated that the small size inferred from the calculations is consistent with other, purely hydrodynamic, applications of the Debye-Brinkman theory. Despite such a shortcoming, the electrokinetic model is robust in its predictive capacity, and it relies on few "unknown" empirical parameters.

The theoretical interpretation of experiment suggests that correlations between microscale segment density and fluid velocity fluctuations significantly influence the effective Stokes radius of the segments. For free and grafted neutral polymer chains, such correlations arise from fluid preferentially flowing through regions of relatively high permeability (low segment density) at scales smaller than those appearing in the Debye-Brinkman model. For terminally anchored polyelectrolyte, at moderate and high ionic strengths when Donnan equilibrium prevails inside the layer, the drag force on the segments is much less susceptible to density fluctuations, and the effective Stokes radius of the segments is representative of their physical size.

A variety of colloids are well known to exhibit anomalous electrokinetic behavior at low ionic strengths. This work did not invoke constructs such as a *dynamic Stern layer* or *charge regulation*. Nevertheless, the present level of detail should assist future studies examining surface chemistry and charge, surface-charge mobility, and the dynamics of adsorbed polymer on fluidlike membranes.

ACKNOWLEDGMENTS

This work was supported by the Natural Sciences and Engineering Research Council of Canada (NSERC) through Grant No. 204542 and the Canada Research Chairs program (Tier II). The author is thankful to Professor D. A. Saville (Princeton University) for helpful suggestions on improving an earlier draft of the manuscript.

[1] R. Galnedar, V. Kahl, A. Arbuzova, M. Rebecchi, J. O. Radler, and S. McLaughlin, Biophys. J. **80**, 2298 (2001).
[2] S. Levine, K. Levine, K. A. Sharp, and D. E. Brooks, Biophys. J. **42**, 127 (1983).
[3] K. A. Sharp and D. E. Brooks, Biophys. J. **47**, 563 (1985).
[4] R. V. McDaniel, K. Sharp, D. Brooks, A. C. McLaughlin, P. Winiski, D. Cafiso, and S. McLaughlin, Biophys. J. **49**, 741 (1986).
[5] J. Janzen, X. Song, and D. E. Brooks, Biophys. J. **70**, 313 (1996).
[6] R. J. Hill, D. A. Saville, and W. B. Russel, J. Colloid Interface Sci. **258**, 56 (2003).
[7] J. A. Cohen and V. A. Khorosheva, Colloids Surf., A **195**, 113 (2001).
[8] J. T. G. Overbeek, Kolloid-Beih. **54**, 287 (1943).
[9] F. Booth, Proc. R. Soc. London, Ser. A **203**, 533 (1950).
[10] P. J. Flory, *Principles of Polymer Chemistry* (Cornell University Press, Ithaca, 1953).
[11] P. G. de Gennes, Macromolecules **13**, 1069 (1980).
[12] D. M. Daoud and J. P. Cotton, J. Phys. (Paris) **43**, 531 (1982).
[13] C. M. Wijmans and E. B. Zhulina, Macromolecules **26**, 7214 (1993).
[14] C. Biver, R. Hariharan, J. Mays, and W. B. Russel, Macromolecules **30**, 1787 (1997).
[15] A. K. Dolan and S. F. Edwards, Proc. R. Soc. London, Ser. A **343**, 427 (1975).
[16] G. J. Fleer, M. A. Cohen Stuart, J. M. H. M. Scheutjens, T. Cosgrove, and B. Vincent, *Polymers at Interfaces* (Chapman and Hall, London, 1988).
[17] S. T. Milner, T. A. Witten, and M. E. Cates, Macromolecules **21**, 2610 (1988).
[18] R. C. Ball, J. F. Marko, S. T. Milner, and T. A. Witten, Macromolecules **24**, 693 (1991).
[19] H. Li and T. A. Witten, Macromolecules **27**, 449 (1994).
[20] H. Orland and M. Schick, Macromolecules **29**, 713 (1996).
[21] N. Dan and M. Tirrel, Macromolecules **25**, 2890 (1992).
[22] G. A. McConnell, E. K. Lin, and A. P. Gast, Faraday Discuss. **98**, 121 (1994).
[23] R. R. Netz and M. Schick, Macromolecules **31**, 5105 (1998).
[24] J. L. Harden, O. V. Borisov, and M. E. Cates, Macromolecules **30**, 1179 (1997).
[25] E. B. Zhulina and O. V. Borisov, J. Chem. Phys. **107**, 5952 (1997).
[26] F. S. Csajka and C. Seidel, Macromolecules **33**, 2728 (2000).
[27] O. V. Borisov, F. A. M. Leermakers, G. J. Fleer, and E. B. Zhulina, J. Chem. Phys. **114**, 7700 (2001).
[28] T. Cosgrove, T. Heath, B. van Lent, F. Leermakers, and J. Scheutjens, Macromolecules **20**, 1692 (1987).
[29] A. Chakrabarti and R. Toral, Macromolecules **23**, 2016 (1990).
[30] K. Binder, P.-K. Lai, and J. Wittmer, Faraday Discuss. **98**, 97 (1994).
[31] S. Rex, M. J. Zuckermann, M. Lafleur, and J. R. Silvius, Biophys. J. **75**, 2900 (1998).
[32] P. S. Doyle, S. G. Shaqfeh, and A. P. Gast, Macromolecules **31**, 5474 (1998).
[33] M. G. Saphiannikova, V. A. Pryamitsyn, and T. Cosgrove, Macromolecules **31**, 6662 (1998).
[34] M. G. Saphiannikova, V. A. Pryamitsyn, and T. M. Birshtein, Macromolecules **33**, 2740 (2000).
[35] W. B. Russel, D. A. Saville, and W. R. Schowalter, *Colloidal Dispersions* (Cambridge University Press, Cambridge, England, 1989).
[36] *Soft Matter Physics*, edited by M. Daoud and C. E. Williams (Springer, Berlin, 1999).
[37] H. J. Ploehn and W. B. Russel, Macromolecules **21**, 1075 (1988).
[38] S. K. Pattanayek and V. Juvekar, Macromolecules **35**, 9574 (2002).
[39] M. A. Cohen Stuart, F. H. W. H. Waajen, T. Cosgrove, B. Vincent, and T. L. Crowley, Macromolecules **17**, 1825 (1984).
[40] G. J. Fleer and J. van Male, Macromolecules **32**, 825 (1999).
[41] G. J. Fleer and J. van Male, Macromolecules **32**, 845 (1999).
[42] H. C. Brinkman, Appl. Sci. Res., Sect. A **1**, 27 (1947).
[43] P. Debye and A. M. Bueche, J. Chem. Phys. **16**, 573 (1948).
[44] A. A. Potanin and W. B. Russel, Phys. Rev. E **52**, 730 (1995).
[45] H. Ohshima, J. Colloid Interface Sci. **163**, 474 (1994).
[46] M. R. Gittings and D. A. Saville, Langmuir **16**, 6416 (2000).
[47] D. A. Saville, J. Colloid Interface Sci. **222**, 137 (2000).
[48] R. W. O'Brien and L. R. White, J. Chem. Soc., Faraday Trans. 2 **74**, 1607 (1978).
[49] C. F. Zukoski and D. A. Saville, J. Colloid Interface Sci. **114**, 32 (1986).
[50] C. F. Zukoski and D. A. Saville, J. Colloid Interface Sci. **114**, 45 (1986).
[51] H. Ohshima, J. Colloid Interface Sci. **130**, 281 (1989).
[52] H. Ohshima, Adv. Colloid Interface Sci. **62**, 189 (1995).
[53] P. W. Atkins, *Physical Chemistry*, 4th ed. (Oxford University Press, Oxford, 1990).
[54] S. Kim and W. B. Russel, J. Fluid Mech. **154**, 269 (1985).
[55] D. L. Koch and A. S. Sangani, J. Fluid Mech. **400**, 229 (1999).
[56] T. G. M. van de Ven, *Colloidal Hydrodynamics* (Academic, San Diego, 1989).
[57] P. G. de Gennes, *Scaling Concepts in Polymer Physics* (Cornell University Press, Ithaca, 1979).
[58] G. D. Smith, *Numerical Solution of Partial Differential Equations*, 3rd ed. (Oxford University Press, Oxford 1985).
[59] M. Eisenberg, T. Gresalfi, T. Riccia, and S. McLaughlin, Biochemistry **18**, 5213 (1979).
[60] J. T. Groves, S. G. Boxer, and H. M. McConnell, Proc. Natl. Acad. Sci. U.S.A. **94**, 13390 (1997).
[61] A. van Oudenaarden and S. G. Boxer, Science **285**, 1046

(1999).
[62] K. Devanand and J. C. Selser, Macromolecules **24**, 5943 (1991).
[63] D. R. Beech and C. Booth, J. Polym. Sci., Polym. Chem. Ed. **7**, 575 (1969).
[64] Y. Takahashi and H. Tadokoro, Macromolecules **6**, 672 (1973).
[65] H. Hasse, H.-P. Kany, R. Tintinger, and G. Maurer, Macromolecules **28**, 3540 (1995).
[66] O. Tirosh, Y. Barenholz, J. Katzhendler, and A. Priev, Biophys. J. **74**, 1371 (1998).
[67] P. L. Hansen, J. A. Cohen, R. Podgornik, and V. A. Parsegian, Biophys. J. **84**, 350 (2003).
[68] *Polymer Handbook*, edited by J. Brandrup, E. H. Immergut, and E.-G. Elias (Wiley, New York, 1966).
[69] P. Bocca, L. Cantu, M. Corti, E. Del Favero, and S. Motta, Langmuir **20**, 2141 (2004).
[70] M. Rovira-Bru, D. H. Thompson, and I. Szleifer, Biophys. J. **83**, 2419 (2002).
[71] P. F. Mijnlieff and F. W. Wiegel, J. Polym. Sci., Polym. Phys. Ed. **16**, 245 (1978).
[72] H. Yamakawa, *Modern Theory of Polymer Solutions* (Harper & Row, New York, 1971).
[73] P. Cottet, H. Gareil, P. Guenoun, F. Muller, M. Delsanti, P. Lixon, J. W. Mays, and J. Yang, J. Chromatogr. A **939**, 109 (2001).
[74] G. S. Manning, J. Chem. Phys. **51**, 924 (1969).